

## **Thick and Thin Films and Submicrometric Scales**



## Some advances in lubrication-type theories

P. Colinet<sup>a</sup>, H. Kaya, S. Rossomme, and B. Scheid

Chemical Engineering Dept., Université Libre de Bruxelles CP 165/67, Avenue F.D. Roosevelt 50,  
1050 Bruxelles, Belgium

**Abstract.** Lubrication-type theories have turned out to be useful in a wide range of scales, being applied to study the dynamics of liquid films of thicknesses ranging between the millimeter and the nanometer. As they moreover allow a deep physical understanding, and are in some cases amenable to analytical treatment, they provide a powerful tool for studying the transition between regimes affected (or even dominated) by inertia, and regimes dominated by contact forces with a solid, for instance. In this paper, recent results of the authors are presented, focusing on thin liquid films flowing down inclines, ultra-thin films of complex fluids featuring density variations, and evaporating contact lines.

### 1 Introduction

Thin films are of great importance in industrial applications such as cooling, lubrication, cleaning, painting, spraying, adhesion, protective coatings, . . . some of these techniques being linked to the rapidly expanding fields of micro-fluidics and nanotechnologies. In some of these thin film applications, it is desirable to maintain a smooth film surface, and it is therefore crucial that the film remains stable over time. However, it is known that liquid films can start to flow, e.g. under the influence of intermolecular forces, with the result that the uniform film sometimes ruptures into a pattern of droplets or holes. In other situations, film deformations are useful, either because they lead to an increased surface area, or because thinner portions of the film present a lower resistance to heat and/or mass transfer, leading to enhanced performances, e.g. for thin-film evaporators. In heat transfer devices based on evaporation such as heat pipes and boilers, contact lines (where a liquid-vapour interface meets a solid) greatly affect the efficiency, since a significant part of the evaporation occurs in their vicinity. In addition to such practical aspects, unanswered fundamental questions are numerous, not only at small scales (limits of validity of continuum models, influence of contact forces, . . .) but also at larger ones (onset of spatio-temporal chaos, transition to turbulence, . . .).

On the modeling side, the thin film geometry permits a separation of longitudinal and transversal length scales in the theoretical analysis of the film dynamics, leading to lubrication-type theories. These theories enable a simplified treatment of thin film systems, enlightening the basic physical phenomena underlying their possibly complex dynamics. Many thin film phenomena are well understood in the framework of lubrication theory (for a review, see Oron, Davis, and Bankoff [1]), but owing to the fundamental and industrial importance of thin films, it has recently become necessary to extend the theory to systems of greater complexity. Without pretending to be exhaustive, we can roughly divide the added complexity into two categories. There is an external complexity contributed by the surroundings of the film and the forces they exert on it, be it heat transfer, air flow, gravity, van der Waals forces, or centrifugal forces created by spinning. Then there is the internal complexity brought in by the internal structure of the liquid that constitutes the film. Where simple fluids are treated as homogeneous

---

<sup>a</sup> e-mail: pcolinet@ulb.ac.be

and incompressible, complex fluids like polymers, liquid crystals, and colloidal suspensions can show internal ordering that is highly affected by the confinement imposed upon them by the thin film geometry. In this article, we would like to present some of our recent advances in applying lubrication-type theories to systems of different kinds, starting from relatively thick films (hundreds of microns) and pursuing on much thinner films (down to a few molecular diameters).

In section 2, the dynamics of a film flowing down an inclined heated surface is described. Such film flows have a rich dynamics extensively studied for a long time since Kapitza's experimental and theoretical pioneering work at the end of the forties [2,3]. Besides their importance for engineering applications (e.g. evaporators or chemical reactors), their interest mainly stems from the fact that their evolution is amenable to thorough theoretical analysis. This situation happens mostly due to the two-dimensional, long-wavelengthed, supercritical character of the primary instability mode. Technically, a lubrication approximation allows the elimination of most of the cross-stream dependence of the flow. The approach is thus similar to that followed in the study of boundary layers and deep analogies can be found in the transition to turbulence of each system, especially at the level of secondary instabilities [4]. For small Reynolds numbers (i.e. small flow rate), where inertia plays only a perturbative role, Benney-type equations for the evolution of the film thickness  $h$  are suitable to describe the dynamics of film flows as reviewed by Oron, Davis and Bankoff [1]. For larger Reynolds number (i.e. larger flow rate) where inertia plays a dominant role, one has to relax the assumption that the velocity field is slaved to the dynamics of film thickness variations. This leads to (integral) boundary layer equations (see e.g. [5]), the most advanced formulation of which has been recently proposed by Ruyer-Quil and Manneville [6,7].

Then, section 3 deals with the effect of internal structure, manifested through density variations, on the stability and dynamics of ultra-thin liquid films under van der Waals forces. The density-variation induced dewetting mechanism proposed by Wensink and Jérôme [8] and by Sharma et al. [9,10] is described, along with our recent treatment of the Marangoni effect brought in by the same density variations [11]. Though the density variation model was originally proposed to describe dewetting phenomena encountered in complex fluid films, recent investigations indicate that deviations from bulk density are not only found in restructuring complex fluids, but may very well also be a general feature of any nanofilm under the influence of van der Waals forces [12–14]. In the vicinity of the interfaces solid-liquid and liquid-gas, intermolecular forces can indeed alter the density from its bulk value [15]. When the film thickness is in the order of a few nanometers, the density of the fluid will deviate from the bulk density throughout the film and not only at the interfaces [12,14]. Some thoughts on the interplay between the fluid structure and external forces and how this can be described in the framework of lubrication-type theories, are put forward.

Finally, section 4 summarizes some recent progress achieved in the understanding of evaporating liquid films and contact lines, for wetting fluids. Similarly to the stress divergence encountered in the moving contact line problem, temperature gradients may also become extremely large in the vicinity of an evaporating contact line, which makes such situation particularly important to understand in order to quantify the evaporation rate of sessile drops, or the growth rate of vapour bubbles on a heater. A number of physico-chemical effects entering into play at such small scales (kinetic resistance to evaporation, van der Waals interactions with the substrate, strong curvatures, . . .), it appears useful to compare their magnitude in order to build sufficiently accurate simplified microscopic models to be incorporated into macroscopic numerical codes.

Some conclusions and perspectives are then outlined in section 5.

## 2 Inertia effects in film flows

We consider first a liquid film flowing down a heated plate inclined by an angle  $\beta$  from the horizontal. In this case, the (Nusselt) flat film state turns out to be unstable to large scale waves, depending on  $\beta$  and other dimensionless numbers characterizing the problem. The separation of

scales enabled by the long wavelength hydrodynamic instability, and quantified by a film parameter  $\varepsilon \ll 1$ , allows to reduce the dimensionality of the basic equations. Prandtl's simplification of the cross-stream momentum equation – usual in boundary layer theory – can be applied here and helps to get rid of the in-depth pressure distribution dominated here by surface tension and gravity. This leads to the so-called boundary-layer equations, see [16] for a detailed presentation. These equations can be viewed as the first step of the long-wave expansion performed by Benney [17]. The modulations of the film thickness around the flat film solution being slow in space and time, it technically consists in applying a gradient expansion to the governing equations through the transformation  $(\partial_t, \partial_x) \rightarrow \varepsilon(\partial_t, \partial_x)$ . Inertia terms, usually multiplied by the Reynolds number, appear thus at order  $\varepsilon$ . The product  $\varepsilon Re$  – where  $Re = g\bar{h}_N^3/3\nu^2$  is the Reynolds number with  $g = g_0 \sin\beta$  the streamwise component of the gravitational acceleration  $g_0$ ,  $\bar{h}_N$  is the Nusselt flat film thickness and  $\nu$  the kinematic viscosity –, is small as in classical lubrication theory. Inertia is thus small and consequently the velocity field remains slaved to the evolution of the film thickness. This leads to a single evolution equation for the film thickness governing the dynamics of the flow, at least near instability onset, which has a conservative form (in the absence of evaporation):

$$\partial_t h + \partial_x \left( q^{(0)} + q^{(1)} + q^{(2)} \right) = 0, \quad (1)$$

where the flow rate  $q = \int_0^h u \, dy$  has been expanded relative to the order of its  $x$ -derivative:

$$\begin{aligned} q^{(0)} &= \frac{1}{3} h^3, \\ q^{(1)} &= \left( \frac{2}{15} h^6 - \frac{1}{3} C h^3 + \frac{MaBi h^2}{2(1+Bi h)^2} \right) \partial_x h + \frac{Ka}{3} h^3 \partial_{xxx} h, \\ q^{(2)} &= \left( \frac{127}{315} h^9 - \frac{8}{15} C h^6 + \frac{7}{3} h^3 + MaBi h^5 \frac{6(5Pr+11) - 5Bi(2Pr-15)h + Bi^2(-7Pr+9)h^2}{120(1+Bi h)^4} \right) \\ &\quad \times (\partial_x h)^2 + \left( \frac{4}{63} h^{10} - \frac{10}{63} C h^7 + h^4 + MaBi h^6 \frac{15Pr+57+Bi(-7Pr+57)h}{240(1+Bi h)^3} \right) \partial_{xx} h, \end{aligned}$$

and where  $Ka = \sigma/\rho\nu^{4/3}g^{1/3}$  (formally assumed of order  $\varepsilon^{-2}$ ),  $C = \cot\beta$ ,  $Ma = \gamma\Delta T/\rho\nu^{4/3}g^{1/3}$  and  $Bi = \alpha\nu^{2/3}/\lambda g^{1/3}$ , with  $\rho$  the density,  $\sigma$  the surface tension and  $\gamma = -d\sigma/dT$  its variation with the temperature,  $\Delta T = T_w - T_a$  the temperature difference between the temperatures of the wall  $T_w$  and of the far-field ambient gas  $T_a$ ,  $\alpha$  the heat transfer coefficient at the liquid-gas interface and  $\lambda$  the thermal conductivity.  $Pr = \nu/\chi$  is the Prandtl number where  $\chi$  is the thermal diffusivity. In this section,  $\Delta T$  is the temperature scale,  $t_\nu = (\nu/g^2)^{1/3}$  the timescale and  $l_\nu = (\nu^2/g)^{1/3}$  is the length scale, hence  $Re = h_N^3/3$  with  $h_N$  the dimensionless film thickness.

Equation (1) has been derived at first order (i.e.  $q^{(2)} = 0$ ) by Joo et al. [18] and is called the *Benney equation* when  $\Delta T = 0$ . The second-order terms increase the accuracy of solutions but decrease the radius of convergence which is limited by a threshold Reynolds number above which finite-time blow-up is observed, as investigated by Scheid et al. [19]. Such a singularity is due to the strong nonlinearity of the inertia term  $\frac{2}{15}\partial_x(h^6\partial_x h)$ , and means that inertia stops to play a perturbative role only balanced by surface tension but plays a dominant role also balanced by the viscous drag.

An alternative to the gradient expansion approach is to make use of the Kármán–Polhausen averaging technique as in the boundary-layer theory [20]. This technique, which was first proposed by Kapitza [2] and later reinvestigated by Shkadov [21], leads in isothermal conditions to a two-field model involving the film thickness  $h$  and the local flow rate  $q$  for which the velocity field is not supposed to be entirely slaved to the film thickness evolution. Even though the Kapitza-Shkadov model has no singularity in the drag-inertia regime, it does not predict the correct instability threshold for surface waves and does not account accurately for inertia effects, mostly due to the assumed parabolic velocity profile. Ruyer-Quil and Manneville have generalized the averaging technique by combining a gradient expansion with a weighted

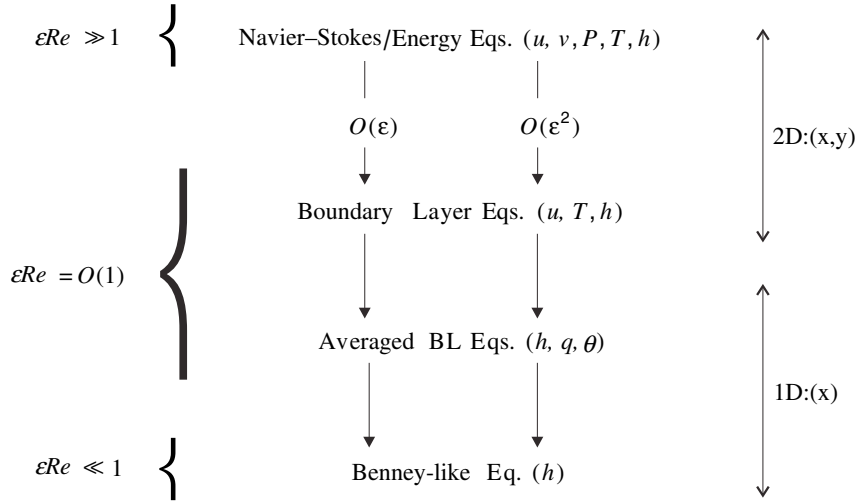


Fig. 1. Hierarchy of models for falling liquid films.

residual method [6,7]. Their model allows for the deviation of the velocity profile from its parabolic shape. For non-isothermal conditions, i.e. with an additional field for the surface temperature  $\theta$ , and accounting for second-order inertia effects, the model reads [22]:

$$\partial_t h = -\partial_x q \quad (2)$$

$$\begin{aligned} \partial_t q = & \frac{9}{7} \frac{q^2}{h^2} \partial_x h - \frac{17}{7} \frac{q}{h} \partial_x q + \left\{ \frac{5}{6} h - \frac{5}{2} \frac{q}{h^2} - \frac{5}{6} Ch \partial_x h + 4 \frac{q}{h^2} (\partial_x h)^2 - 6 \frac{q}{h} \partial_{xx} h - \frac{9}{2h} \partial_x q \partial_x h \right. \\ & \left. + \frac{9}{2} \partial_{xx} q - Ma \left( \frac{5}{4} \partial_x \theta - \frac{1}{224} h q \partial_{xx} \theta \right) + \frac{5}{6} Kah \partial_{xxx} h \right\} \\ & \times \left( 1 - \frac{1}{70} q \partial_x h + Ma \frac{5}{56} \frac{\partial_x \theta}{h} \right)^{-1} \end{aligned} \quad (3)$$

$$\begin{aligned} Pr \partial_t \theta = & 3 \frac{(1 - \theta - Bih\theta)}{h^2} + Pr \left[ \frac{7}{40} \frac{(1 - \theta)}{h} \partial_x q - \frac{27}{20} \frac{q}{h} \partial_x \theta \right] + (1 - \theta - \frac{3}{2} Bih\theta) \frac{(\partial_x h)^2}{h^2} \\ & + \frac{\partial_x h \partial_x \theta}{h} + (1 - \theta) \frac{\partial_{xx} h}{h} + \partial_{xx} \theta \end{aligned} \quad (4)$$

The validity range of this model extends to moderate Reynolds numbers, i.e.  $\varepsilon Re = O(1)$  but by construction, a gradient expansion of it leads back to the Benney-type equation (1) only valid for  $\varepsilon Re \ll 1$ . The different levels of simplification (i.e. lubrication-type approximations) from the Navier–Stokes/Energy equations can now be summarized in figure 1, along with on the left, the domain of validity, and on the right the dimensionality of the different models (ignoring spanwise variations here). Notice also in figure 1 the two vertical axes indicating that each model can be written at first or second order in terms of the film parameter  $\varepsilon$ : the  $O(\varepsilon)$ -models turn out to be suitable for fluids with large surface tension, i.e.  $Ka = O(10^3 - 10^4)$ , like water or glycerin flowing along a vertical wall or the flow of almost any fluid for very slight inclination (since  $Ka \propto \sin \beta^{-1/3}$ ), while the  $O(\varepsilon^2)$ -models should be considered when the streamwise viscous dissipation becomes important as compared to surface tension, i.e.  $Ka = O(10 - 10^2)$ , like ethyl alcohol flowing along a vertical wall. One should keep in mind that figure 1 is valid for non-isothermal conditions only for  $Pr = O(1)$ .

Figure 2 shows dispersion curves obtained from the linear stability analysis of the Nusselt flat film solution for each model classified in figure 1 (see details in [23]). It clearly shows the agreement of all models for small Reynolds numbers ( $Re = 1$ ) but the divergence of the growth rate predicted by the Benney-like equation for larger Reynolds number ( $Re = 10$ ) while the

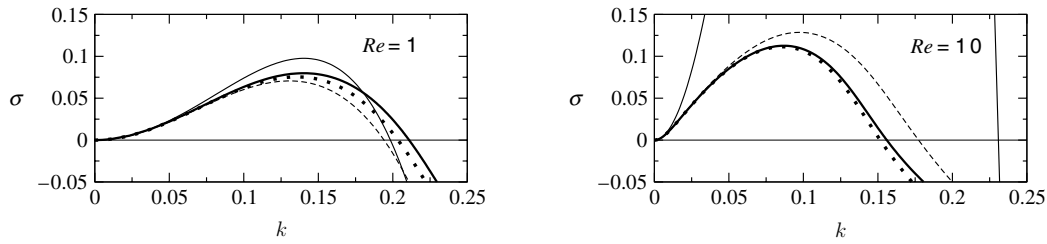


**Fig. 2.** Growth rate  $\sigma$  versus wavenumber  $k$  for various  $Re$  and obtained from the Navier-Stokes/Fourier equations (thick solid lines), the boundary layer equations (dotted lines), the averaged equations (dashed lines) and the Benney-like equation (thin solid lines), for  $Ka = 250$ ,  $Pr = 7$ ,  $Ma = 50$  and  $Bi = 1$ .

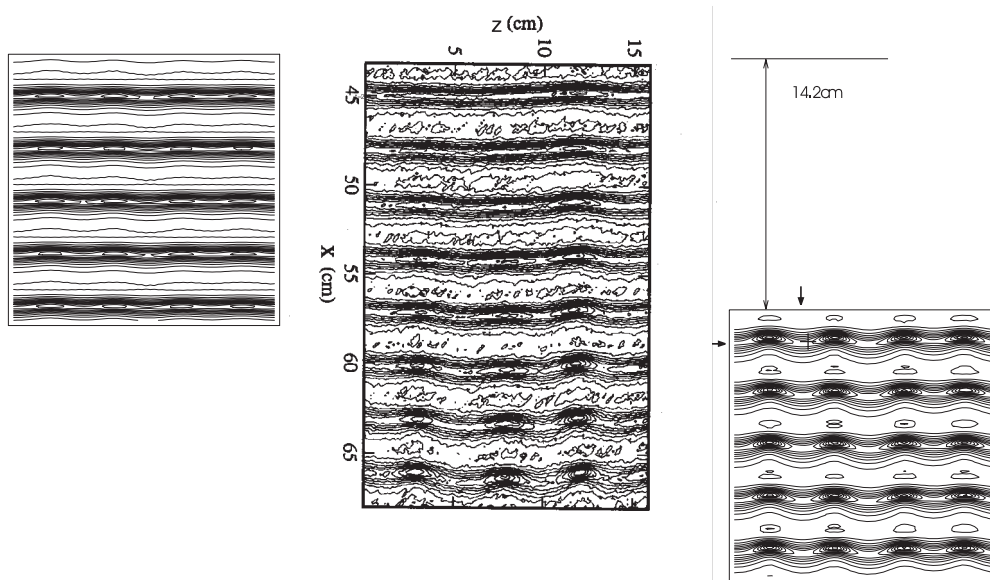


**Fig. 3.** Simulation results (on the sides) of the isothermal and 3D version of equations (2)–(4) with  $Re = 42.7$ ,  $Ka = 2340$ ,  $C = 14.3$  and  $Ma = 0$ . The middle picture shows the experimental result by Liu et al. 1995, figure 7 (reprinted from [24], figure 15). Isothickness contours are separated by an elevation step of  $0.06$  (corresponding to  $60 \mu m$ ). The location of a saddle point in the right snapshot is indicated by a cross and two arrows.

predictions with the averaged equations remain in good agreement with the original balance equations.

In the nonlinear three-dimensional regime, averaged equations have also shown their ability to accurately describe wave patterns in thin film flows as demonstrated by Scheid, Ruyer-Quil and Manneville [24]. One of the most remarkable breakthrough has been to recover the synchronous pattern observed in experiments by Liu, Schneider and Gollub [25] and illustrated in figure 3. This is due to the proper formulation of second-order inertia effects using a Padé-like regularization procedure that yields the denominator in (3). Experiments and simulations share common qualitative features. Isothickness contours agree well with each other, and strong spanwise modulations of the troughs are observed, whereas the crests remain nearly undeformed, which leads to the formation of isolated depressions. In particular, as experimentally observed by Liu et al., the numerical simulations here indicate the occurrence of local saddle points on the wave pattern corresponding to maxima in the spanwise direction and minima in the streamwise direction.

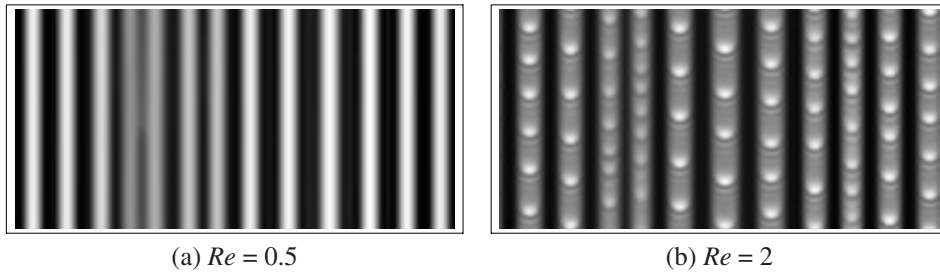


**Fig. 4.** Simulation results of the 3D version of equations (2)–(4) with  $Ka = 3375$ ,  $C = 0$ ,  $Pr = 7$ ,  $Ma = 25$  and  $Bi = 0.1$ . Bright (dark) zones correspond to elevations (depressions).

Figure 4 shows the last stage before rupture of the numerical simulations of a water film at  $20^\circ\text{C}$  flowing down a vertical heated wall. The figure reveals the presence of rivulet structures formed due to the Marangoni effect. For small Reynolds number ( $Re = 0.5$ ) the regularly spaced rivulets aligned in the streamwise direction prevent the development of hydrodynamic waves. Such a structure has been first observed experimentally by Ludviksson and Lightfoot [26], predicted by Goussis and Kelly [27] and simulated by Joo et al. [28] using a 3D version of equation (1) truncated at first order. For larger Reynolds number ( $Re = 2$ ), i.e. outside the range of validity of the single evolution equation (1) for the film thickness, we observed a complex cooperative behavior for the hydrodynamic and thermocapillary modes with the presence of rivulets fostering quasi-two-dimensional waves of larger amplitude and phase speed than those observed in isothermal conditions, leading possibly to solitary-like waves. A systematic study of such phenomena will be addressed in a future work.

### 3 Effect of density variations on ultrathin film stability

Considering now films with a much smaller thickness, down to nanoscale, it is necessary to account for the fact that the constituent molecules will experience different conditions than in a bulk liquid. The close proximity of the neighbouring phases induces van der Waals forces that act not only in the interfacial regions, but throughout the film. These van der Waals forces are due to intermolecular dipole forces, and their magnitude can be calculated from the polarizabilities of the involved media [29], which in the basic case would be the film, the supporting substrate and the gas phase above the film. The film molecules also interact between themselves, and in a thin film geometry, the interaction symmetry that the molecules experience in the bulk state, is broken.

Assuming pairwise interactions and homogeneous media, it is straightforward to sum all the interactions acting on the film by integrations. Starting from the long-range, attractive part of a Lennard-Jones potential, the total free energy per unit area turns out to have an excess term for finite film thicknesses, reading

$$e(h) = \frac{A_{\text{SFG}}}{12\pi h^2}, \quad (5)$$

where  $A_{\text{SFG}}$  is the Hamaker constant, which depends on the molecular polarizabilities and densities in the phases S(olid), F(ilm), and G(as). Evidently,  $A_{\text{SFG}} > 0$  means that thick, stable films are energetically favoured. Conversely,  $A_{\text{SFG}} < 0$  means that the excess energy is reduced when the film grows thinner, thus promoting film destabilization and rupture.

More generally, when  $e(h)$  is a concave function of  $h$  (i.e.  $e''(h) < 0$ ), the film surface will form deformation patterns that grow in amplitude and eventually form a pattern of regularly spaced droplets. This rupture mechanism is known as spinodal dewetting and is triggered by any disturbance of the uniform film surface, regardless the amplitude. The other important rupture mechanism, nucleation, occurs when  $e(h)$  displays a barrier, which would require a more complex expression than (5). The film may then be metastable, so that rupturing will take place when a disturbance has a sufficiently high amplitude. In this case, rupture will not

lead to a global pattern of droplets, but typically to localized holes, nucleated at impurities or imperfections of the substrate.

The excess energy (5) gives rise to an excess pressure acting on the film, known as the *disjoining pressure* and defined by

$$\Pi(h) = -\frac{\partial e}{\partial h} = \frac{A_{\text{SFG}}}{6\pi h^3}. \quad (6)$$

The disjoining pressure is derived as a pressure acting between two parallel, flat interfaces. It is common practice to keep treating it this way, even if the film thickness exhibits lateral variations. This is the celebrated Derjaguin approximation [30], which is closely related to the lubrication approximation in treating these lateral variations as sufficiently slow in space.

Recently, several authors have addressed the effects that variations in the density of the film have on its stability [8–11]. The Hamaker constant  $A_{\text{SFG}}$  depends on the particle number densities in the phases S, F, G. Variations in the densities thus create additional terms in the disjoining pressure. In a bulk fluid, local variations in the fluid density can be ignored upon taking the thermodynamic limit for the number of molecules and the dimensions of the system. For a thin film, however, the transversal dimension is dramatically restricted. For nanofilms, the film thickness corresponds to a few molecular diameters. A nanofilm is thus a thermodynamically small system in which the effect of fluctuations should be properly accounted for.

The effect of density variations emerges especially in nanofilms of complex fluids. Polymers and liquid crystals confined in a thin film geometry by rapid preparation methods like spin coating will be in non-equilibrium configurations. As the molecules restructure to attain their equilibrium configurations, density variations will occur, which have a long life-time due to the slow dynamics of complex fluids. If these density variations are sustained for a sufficiently long time, they may destabilize the film.

The possibly most rigorous approach to density variations in a thin liquid film treated as a continuous medium is the diffuse interface theory [12]. An important concept in this theory is the introduction of a capillary tensor created by density gradients inside the liquid.

Here, however, we stick to a simpler approach. Treating the density variations as weak, we use a Boussinesq-like approximation and ignore the density variations except when they couple to external fields, in this case represented by the van der Waals forces and the surface tension. The resulting effects on the thin film flow and stability occur through the modification of the disjoining pressure forces and the density-induced Marangoni flow.

Applying lubrication theory to the governing system of hydrodynamic equations (neglecting inertia here), the dimensionless evolution equation for the thin film reads

$$\partial_T H + \nabla \cdot \left[ \frac{H^3}{3} \nabla (\nabla^2 H + \Phi) + \text{Ma} \frac{H^2}{2} \partial_H \Gamma_s \nabla H \right] = 0, \quad (7)$$

where the dimensionless disjoining pressure  $\Phi$  is given by

$$\Phi = \frac{\text{Wa} + \Gamma(H)\text{Wd}}{H^3}. \quad (8)$$

The dimensionless density  $\Gamma(H) = (\rho(h) - \rho_b) / (\rho_i - \rho_b)$  is a measure of the local mean liquid density  $\rho(h(x, y))$  relative to the bulk density  $\rho_b$  and a density  $\rho_i$  defined to be the value at  $h \rightarrow 0$ , i.e. at infinite confinement. A constitutive relation relating  $\rho$  to  $h$  is needed, and as a simple model a Padé function interpolating  $\rho_b$  and  $\rho_i$  is used, giving  $\rho(h) = \rho_b + (\rho_i - \rho_b) (1 + bh)^{-1}$ , defining the rate of density change  $b$  as an additional parameter. The dimensionless density function then reads  $\Gamma(H) = (1 + BH)^{-1}$ , where  $B = bh_0$  is the density change rate scaled by the average film thickness  $h_0$ .

By a considered choice of characteristic time and length scales in the non-dimensionalization, the thin film model can be analysed by means of three parameters only. The van der Waals number  $\text{Wa}$  only plays the role of a “flag”, taking the value  $\pm 1$ , the sign indicating whether the film is spinodally stable or unstable at bulk density. Only the van der Waals gradient number  $\text{Wd} = (\rho_i - \rho_b) \partial_\rho A|_{\rho=\rho_b} / |A_{\rho=\rho_b}|$ , the dimensionless density change rate  $B$ , and the

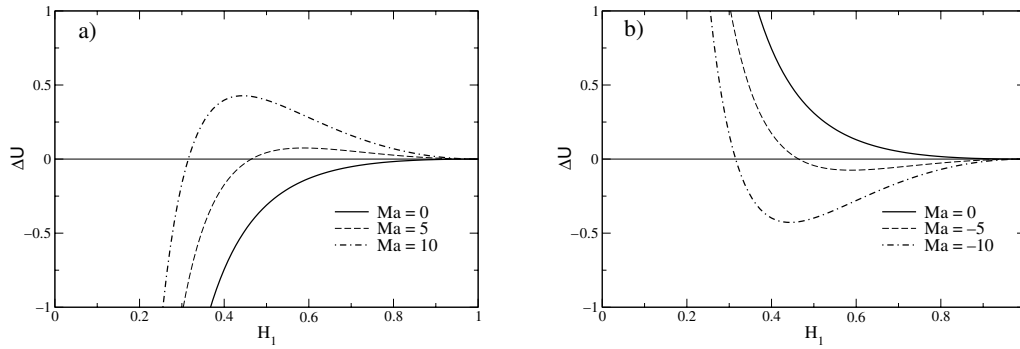


**Fig. 5.** Effect of  $Ma$  on the film stability. a) A thermodynamically stable film ( $Wa = 1$ ) with destabilizing density variations ( $Wd = -2$ ,  $B = 1$ ). Increasing  $Ma$ , the film goes from being unstable ( $Ma = 0$ ) to metastable. b) A thermodynamically unstable film ( $Wa = -1$ ) with stabilizing density variations ( $Wd = 2$ ,  $B = 1$ ). Decreasing  $Ma$ , the film goes from being stable ( $Ma = 0$ ) to pseudo-unstable.

Marangoni number  $Ma = 6\pi h_0^2(\rho_i - \rho_b)\partial_\rho\sigma|_{\rho=\rho_b}/|A_{\rho=\rho_b}|$  are free to vary. In these expressions,  $A(\rho)$  and  $\sigma(\rho)$  are the density-dependent Hamaker constant and surface tension, respectively. Note that in equation (7), a dimensionless surface concentration  $\Gamma_s$  has been introduced in the Marangoni term. Another constitutive expression is therefore needed, which will here be selected as  $\Gamma_s(H) = (1 + BH)^{-2} < \Gamma(H)$ , hence reflecting the fact that surface molecules have more freedom to relax to their equilibrium configurations than in the bulk.

With the addition of the  $H$ -dependent term in the numerator, equation (8) becomes qualitatively similar to the disjoining/conjoining pressure terms used in the study of thin films on layered substrates [31], or, equivalently, the attractive-repulsive potential used to account for Born repulsion at ultrathin film thicknesses [32,33] and to avoid the singularities that application of the long-range term alone unavoidably will evoke as the film thickness approaches zero. However, the additional, density-dependent term in equation (8) does not necessarily play such a strictly stabilizing role. Given the values of  $Wa$  and  $Wd$ , it can act both destabilizing [8] and stabilizing [9].

The linear stability analysis shows that applying the Boussinesq approximation does not change the physical behaviour of the model compared to the general case studied in [11], except for the time scales. Sufficiently strong density variations can change the sign of the numerator in (8) and render a stable film unstable, and vice versa. This was shown in earlier works on the density variation model. In addition, however, nonlinear energy analysis reveals that the combined effect of Marangoni flow and density gradients can make the film metastable and pseudo-unstable, as illustrated by the energy curves in figure 5. They plot the work necessary (per unit area) to create a large hole in which the film thickness is  $H_1$  [34]. Metastability can cause local rupture in a flat film by nucleation, whereas pseudostability refers to a film where the flat state is unstable, but where a potential barrier ultimately prevents rupturing of the film. This case is shown in figure 6.

On a final note in this section, it is reasonable to ask if lubrication theory derived from hydrodynamic continuum equations is applicable to nanoscale phenomena. Another reasonable reservation is the use of newtonian viscosity law to model complex fluids. The latter problem is currently being addressed by introducing viscoelastic models to the thin film equation [35,36]. The agreement between AFM-measured topologies and hydrodynamic equations demonstrated in [37] seems to support the validity of the continuum approach down to the nanoscale.

## 4 Evaporating films and contact lines

Ignoring any density variation but adding the possible evaporation of the thin (or ultra-thin) film, we consider in this section that the latter is bounded above by its own vapour and below by a uniformly heated solid plate (see figure 7).  $\mathcal{J}(x, y, t)$  is the interfacial mass flux,  $T^\nabla$  is the

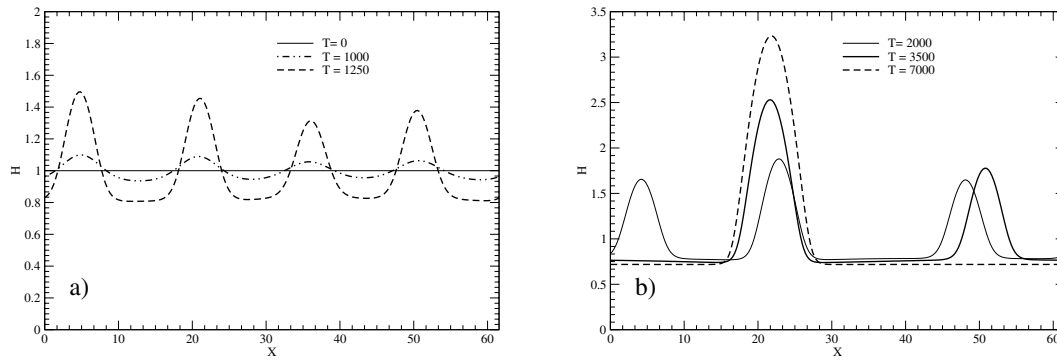


**Fig. 6.** a) A thermodynamically unstable film ( $Wa = -1$ ) exhibiting pseudo-dewetting due to the stabilizing influence of density variations and Marangoni flow ( $Wd = 4$ ,  $B = 2$ ,  $Ma = -10$ ). b) Long-time coalescence and coarsening of the droplets.

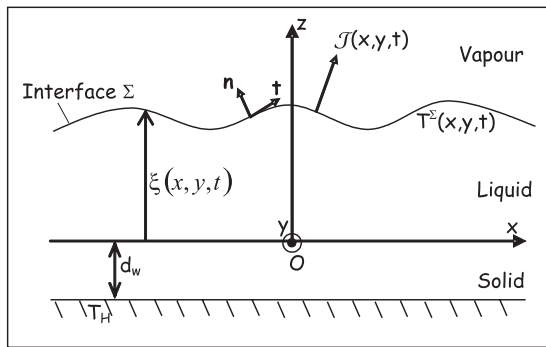


**Fig. 7.** The system is composed of a rigid substrate on which lies a completely wetting volatile liquid film. The latter is in contact with its own vapour at the interface  $z = \xi(x, y, t)$ .

temperature of the liquid-vapour interface, and  $T_H$  is the constant temperature of the heated plate at  $z = -d_w$  (with  $d_w$  the thickness of the solid).

As various physico-chemical processes may influence the dynamics of such a liquid film (e.g. interfacial kinetics of evaporation, vapour recoil, thermocapillarity, disjoining pressure, ...), it is important to quantify their relative magnitude, which is most easily achieved on the basis of a lubrication-type equation. The latter here reads

$$\partial_t \xi + E\mathcal{J} + \nabla \cdot \mathbf{q} = 0,$$

$$\mathbf{q} = \frac{-A}{\xi} \nabla \xi + S\xi^3 \nabla (\nabla^2 \xi) - \mathcal{M}\xi^2 \nabla (c_l + g_l \xi) - \mathcal{D}\mathcal{J}\xi^3 \nabla \mathcal{J}, \quad (9)$$

which shows that the temporal evolution of the thickness  $\xi$  is due to the evaporative mass loss, together with the usual divergence of a flux  $\mathbf{q}$ , here driven by disjoining pressure  $p_d = A\xi^{-3}$ , capillary pressure  $p_\sigma = -3S\Delta\xi$ , thermocapillarity and vapour recoil. In this section, the dimensionless numbers are  $E = \lambda\Delta T/\rho\nu\mathcal{L}$ ,  $A = A_{\text{SFG}}/\rho\nu^2\xi_0$ ,  $S = \sigma\xi_0/3\rho\nu^2$ ,  $\mathcal{M} = \gamma\Delta T\xi_0/2\rho\nu$  and  $\mathcal{D} = 2E^2\rho/3\rho_v$ . In these expressions, usual notations are used for fluid properties (see previous sections), with in addition  $\mathcal{L}$  for the latent heat of evaporation and  $\rho_v$  for the vapour density. Moreover,  $\xi_0$  is an arbitrary thickness and  $\Delta T = T_H - T_{\text{sat}}(p_v)$ , i.e. the temperature difference between the underside of the substrate and the saturation temperature  $T_{\text{sat}}$  at given vapour pressure  $p_v$ . Note that quantities  $g_l$  and  $c_l$  are defined hereafter.

Importantly, even though the structure of the evolution equation (9) is identical to that found by Burelbach et al. [38], for ultra-thin films it is crucial to incorporate the effect of van der Waals interactions with the substrate in the calculation of the evaporation flux  $\mathcal{J}$ .

This indeed allows to obtain adsorbed films and to study evaporation near a contact line (see hereafter), as shown by Stephan and Busse [39], though these authors restricted their analysis to steady solutions, and neglected several effects considered here. A more recent work of Ajaev

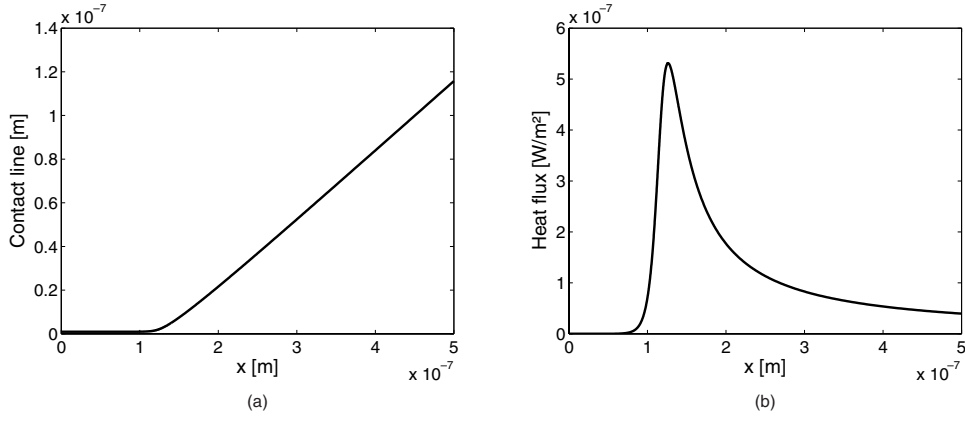


**Fig. 8.** Thickness profile and corresponding evaporative heat flux for ammonia at  $T_{sat} = 300$  K, submitted to a superheat  $\Delta T = T_H - T_{sat} = 1$  K, and with  $R_s = \mathcal{M} = 0$ .

[40] is similar to the present model in many respects, though its main goal was to study the influence of evaporation on liquid flow down a heated inclined surface, rather than to focus on details of the heat flux near a contact line such as done here.

Specifically, ignoring heat conduction in the vapour for simplicity, still considering a possible thermal resistance  $R_s = d_w \lambda / \lambda_w \xi_0$  of the solid wall (where  $d_w$  and  $\lambda_w$  are its thickness and thermal conductivity, respectively), the dimensionless liquid temperature gradient  $g_l$ , the solid-liquid interface temperature  $c_l$  and the evaporation flux  $\mathcal{J}$  are found as

$$g_l = \frac{\phi\Omega - 1}{R_s + K + \xi}, \quad c_l = \frac{K + \xi + R_s\phi\Omega}{R_s + K + \xi}, \quad \mathcal{J} = -g_l = \frac{1 - \phi\Omega}{R_s + K + \xi}, \quad (10)$$

where  $\Omega = p_d - p_\sigma = A\xi^{-3} + 3S\Delta\xi$ ,  $\phi = T_{sat}\nu^2 / \mathcal{L}\Delta T\xi_0^2$ , and  $K = \lambda T_{sat}^2 / L_{ww}\xi_0\mathcal{L}^2$  (here,  $L_{ww}$  is a phenomenological proportionality coefficient between the evaporation rate and the chemical potential difference across the interface).

Expressions (10) include the variation of liquid chemical potential with both disjoining and capillary pressure, which actually result in a dependence of the local saturation temperature upon these quantities (deviation with respect to the Clausius-Clapeyron law  $T_{sat}(p_v)$ , restricted to a flat interface outside the range of molecular interactions with a solid). These effects are quantified by the dimensionless parameter  $\phi$ , while the kinetic resistance to evaporation is measured by the parameter  $K$ .

Equation (9) admits a stationary flat film solution, which results from the balance between the evaporation driving force and the attractive intermolecular interactions with the solid. From equation (10), the thickness of such adsorbed (or precursor) film is found as  $\xi_0^* = \sqrt[3]{A\phi}$ , whose stability can also be studied within the framework of equation (9). Even though this adsorbed film could be destabilized at a certain critical Marangoni number, the actual value calculated for typical fluids turns out to be much smaller than the latter, i.e. the adsorbed film is always stable in practice.

Contact lines can then be constructed as mesoscopic regions connecting such a microscopic film to a “macroscopic” region, though the latter should here be considered as such merely in the asymptotic sense. An example of such steady solution of the one-dimensional version of equation (9) is shown in figure 8(a).

Importantly, the evaporation flux  $\mathcal{J}$  is generally non-zero for solutions connecting the adsorbed film to a macroscopic region of vanishingly small curvature, as seen in figure 8(b). Clearly, the contact angle measured is a non-equilibrium contact angle, resulting from a dynamic balance between evaporation and wetting, which as said above, is assumed to be complete here. As such, the value of this apparent contact angle is generally found to increase with the evaporation rate, which may be varied, for instance, by controlling the superheat  $\Delta T = T_H - T_{sat}$  (see figure 9).

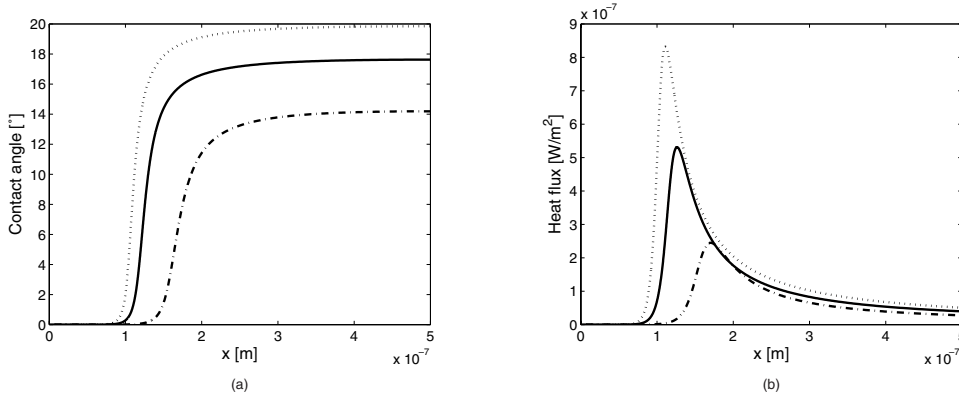


**Fig. 9.** Local contact angle (slope profile) and corresponding evaporative heat flux for ammonia at  $T_{sat} = 300$  K,  $R_s = \mathcal{M} = 0$ , for various  $\Delta T = T_H - T_{sat}$ :  $\Delta T = 0.5$  K (dot-dashed lines),  $\Delta T = 1$  K (solid lines),  $\Delta T = 1.5$  K (dotted lines).

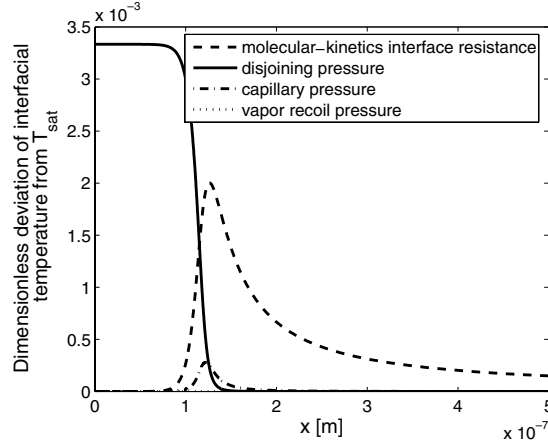


**Fig. 10.** The different contributions (in units of  $T_{sat} = 300$  K) to the dimensionless deviation of the interfacial temperature from  $T_{sat}$ , for ammonia and a superheat of  $\Delta T = 1$  K.

As seen in figures 8(b) and 9(b), the local heat flux presents a strong peak at the location of the apparent contact line, as emphasized by Stephan and Busse [39]. Clearly, the heat flux at the contact line would even diverge if there were no adsorbed film and no deviation of the interfacial temperature from  $T_{sat}$  (approaching the contact line, the thermal gradient would grow as  $(T_H - T_{sat})/\xi$ , if the solid is perfectly conducting). This divergence, which is analogous to the stress divergence in the moving contact line problem, is here regularized by considering both an adsorbed film and deviations of the interface temperature with respect to  $T_{sat}$ . Actually, in dimensionless form (measuring temperatures from  $T_{sat}$  and using  $\Delta T$  as temperature scale), the kinetic law used here may be written

$$T^\Sigma = \phi\Omega + K\mathcal{J} = \phi(A\xi^{-3} + 3S\xi'') + K\mathcal{J}, \quad (11)$$

indicating that the interfacial temperature deviates from  $T_{sat}$  due to disjoining and capillary pressures, in addition to the intrinsic kinetic resistance to evaporation (inversely proportional to the accommodation coefficient in Hertz-Knudsen law). The relative magnitude of these effects is compared in figure 10, together with the effect of vapour recoil pressure which may in principle also be included in equation (11). However, the latter is found to be negligible for all cases considered here.

It is found that the disjoining pressure entirely determines the interfacial temperature deviation in the adsorbed film region, while the kinetic resistance to evaporation plays the

major role at larger scales. In the macroscopic domain, the interface sticks to the saturation temperature, however. In the high-curvature mesoscopic region, the capillary pressure may also turn to be significant. A last peak-smoothing effect is clearly the thermal resistivity of the solid  $R_s$  (acting quite similarly to the slip length for the moving contact line problem), whose effect may be readily compared to the kinetic interfacial resistance  $K$  on the basis of equations (10).

Numerical simulations of equation (9) have been carried out in order to estimate the influence of the other physical effects on the contact angle and on the evaporation flux. As said above, the vapour recoil pressure does not have any influence in the conditions selected here, and it can be safely neglected. On the other hand, the heat flux decreases when the thermal resistance of the solid and the kinetic resistance to evaporation increase. While the contact angle is found to decrease in the same conditions, it may slightly increase with the Marangoni number, even though the heat flux is found to decrease in this case.

## 5 Conclusions and perspectives

Some applications of lubrication theory to different thin film systems have been presented, both for relatively thick films flowing along an inclined plane, and for much thinner films influenced by intermolecular interactions with the surrounding phases. As far as thick films are concerned, taking inertia into account requires accurate multi-equation models to be considered, still computationally advantageous over full-scale numerical simulations of original momentum and energy balances in a time-dependent domain. Clearly, having such reliable low-dimensional models at our disposal will allow to attack many pattern-forming issues still open for plain film flows over inclined planes, including more difficult cases involving heat transfer. As far as ultra-thin liquid films are concerned, although the proposed model appears in qualitative agreement with earlier experiments, an important future goal will be to improve the treatment of density fluctuations, possibly by taking into account their dynamics through a second evolution equation [41]. Finally, lubrication-type models have been shown to be adequate in modeling the dynamics and heat transfer near contact lines, provided an adsorbed (or precursor) film exists, which can be naturally taken into account in case the liquid is treated as volatile. In this case, it is worth pointing out that other effects might also be important to incorporate in the analysis, such as temperature discontinuities across the interface [42], inert gases [43], and geometrical or chemical heterogeneities of the substrate [29].

The authors gratefully acknowledge financial support of the Fonds de la Recherche Scientifique – F.N.R.S. of the Communauté Française de Belgique through the ARCHIMEDES project (ARC 04/09-308), of the Fonds pour la Formation à la Recherche dans l’Industrie et l’Agriculture, and of the PRODEX Programme managed by the European Space Agency in collaboration with the Belgian Federal Science Policy Office.

## References

1. A. Oron, S.H. Davis, S.G. Bankoff, *Rev. Mod. Phys.* **69**, 931 (1997)
2. P. Kapitza, *Zh. Ekper. Teor. Fiz.* **18**, 3 (1948)
3. P. Kapitza, S. Kapitza, *Zh. Ekper. Teor. Fiz.* **19**, 105 (1949)
4. T. Herbert, *Ann. Rev. Fluid Mech.* **20**, 487 (1988)
5. S. Alekseenko, V. Nakoryakov, B. Pokusaev, *Wave Flow in Liquid Films* (Begell House, NY, 1994)
6. C. Ruyer-Quil, P. Manneville, *Eur. Phys. J. B* **15**, 357 (2000)
7. C. Ruyer-Quil, P. Manneville, *Phys. Fluid* **14**, 170 (2002)
8. K.D.F. Wensink, B. Jérôme, *Langmuir* **18**, 413 (2002)
9. A. Sharma, J. Mittal, *Phys. Rev. Lett.* **89**, 186101 (2002)
10. A. Sharma, J. Mittal, R. Verma, *Langmuir* **18**, 10213 (2002)
11. H. Kaya, B. Jérôme, P. Colinet, *Europhys. Lett.* **74**, 861 (2006)
12. L.M. Pismen, Y. Pomeau, *Phys. Rev. E* **62**, 2480 (2000)
13. L.M. Pismen, *Phys. Rev. E* **64**, 021603 (2001)

14. S. Gavriluk, I. Akhatov, Phys. Rev. E **73**, 021604 (2006)
15. H. Gouin, J. Phys. Chem. B **102**, 1212 (1998)
16. H.-C. Chang, E. Demekhin, D. Kopelevitch, J. Fluid Mech. **250**, 433 (1993)
17. D. Benney, J. Math. Phys. **45**, 150 (1966)
18. S.W. Joo, S.H. Davis, S.G. Bankoff, J. Fluid Mech. **230**, 117 (1991)
19. B. Scheid, C. Ruyer-Quil, U. Thiele, O. Kabov, J.C. Legros, P. Colinet, J. Fluid Mech. **527**, 303 (2005)
20. H. Schlichting, *Boundary-Layer Theory* (McGraw-Hill, 1979)
21. V. Shkadov, Izv. Ak. Nauk SSSR, Mekh. Zhidk Gaza **1**, 43 (1967)
22. C. Ruyer-Quil, B. Scheid, S. Kalliadasis, M.G. Velarde, R.Kh. Zeytounian, J. Fluid Mech. **538**, 199 (2005)
23. B. Scheid, C. Ruyer-Quil, S. Kalliadasis, M.G. Velarde, R.Kh. Zeytounian, J. Fluid Mech. **538**, 223 (2005)
24. B. Scheid, C. Ruyer-Quil, P. Manneville, J. Fluid Mech. **562**, 183 (2006)
25. J. Liu, J. Schneider, J. Gollub, Phys. Fluids **7**, 55 (1995)
26. V. Ludviksson, E.N. Lightfoot, AIChE J. **14**, 620 (1968)
27. D.A. Goussis, R.E. Kelly, J. Fluid Mech. **223**, 25 (1991)
28. S.W. Joo, S.H. Davis, S.G. Bankoff, J. Fluid Mech. **321**, 279 (1996)
29. P.G. de Gennes, F. Brochard-Wyart, D. Quéré, *Gouttes, bulles, perles et ondes* (Belin, Paris, 2002)
30. B.V. Derjaguin, Kolloid Z. **69**, 155 (1934)
31. A. Oron, S.G. Bankhoff, J. Coll. Interf. Sci. **218**, 152 (1999)
32. V. Mitlin, J. Coll. Interf. Sci. **153**, 491 (1993)
33. A.L. Bertozzi, G. Grün, T.P. Witelski, Nonlinearity **14**, 1569 (2001)
34. V. Mitlin, J. Colloid Interface Sci. **227**, 371 (2000)
35. S. Herminghaus, K. Jacobs, R. Seemann, Eur. Phys. J. E **12**, 101 (2004)
36. M. Rauscher, A. Münch, B. Wagner, R. Blossey, Eur. Phys. J. E **17**, 373 (2005)
37. J. Becker, G. Grün, R. Seemann, H. Mantz, K. Jacobs, K.R. Mecke, R. Blossey, Nature Mater. **2**, 59 (2003)
38. J.P. Burelbach, S.G. Bankoff, S.H. Davis, J. Fluid Mech. **195**, 463 (1988)
39. P.C. Stephan, C.A. Busse, Int. J. Heat Mass Transfer **35**, 383 (1992)
40. V.S. Ajaev, J. Coll. Interface Sci. **280**, 165 (2004)
41. U. Thiele, Eur. Phys. J. E **12**, 409 (2003)
42. G. Fang, C.A. Ward, Phys. Rev. E **59**, 417 (1999)
43. B. Haut, P. Colinet, J. Coll. Interface Sci. **285**, 296 (2005)

